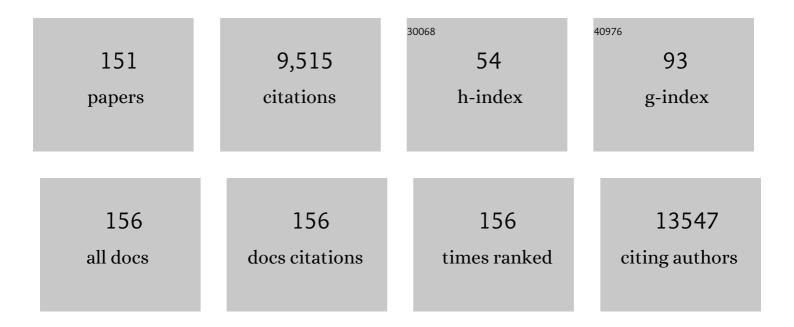
List of Publications by Year in descending order

Source: https://exaly.com/author-pdf/2416731/publications.pdf Version: 2024-02-01



Ρορινίι

#	Article	IF	CITATIONS
1	Ultrasensitive NO <sub>2</sub> Gas Sensors Based on Layered αâ€MoO <sub>3</sub> Nanoribbons. Advanced Materials Technologies, 2022, 7, 2100579.	5.8	13
2	Ru(bpy)32+-sensitized {001} facets LiCoO2 nanosheets catalyzed CO2 reduction reaction with 100% carbonaceous products. Nano Research, 2022, 15, 1061-1068.	10.4	24
3	Interpolation between W Dopant and Co Vacancy in CoOOH for Enhanced Oxygen Evolution Catalysis. Advanced Materials, 2022, 34, e2104667.	21.0	45
4	hcp-phased Ni nanoparticles with generic catalytic hydrogenation activities toward different functional groups. Science China Materials, 2022, 65, 1252-1261.	6.3	5
5	Scalable Spray Drying Production of Amorphous V <sub>2</sub> O <sub>5</sub> –EGO 2D Heterostructured Xerogels for Highâ€Rate and High apacity Aqueous Zinc Ion Batteries. Small, 2022, 18, e2105761.	10.0	24
6	TMN4 complex embedded graphene as efficient and selective electrocatalysts for chlorine evolution reactions. Journal of Electroanalytical Chemistry, 2022, 907, 116071.	3.8	16
7	β-Arsenene Monolayer: A Promising Electrocatalyst for Anodic Chlorine Evolution Reaction. Catalysts, 2022, 12, 296.	3.5	3
8	Hydrogen Spillover-Bridged Volmer/Tafel Processes Enabling Ampere-Level Current Density Alkaline Hydrogen Evolution Reaction under Low Overpotential. Journal of the American Chemical Society, 2022, 144, 6028-6039.	13.7	179
9	Low-Dimensional Metal–Organic Frameworks with High Activity and Selectivity toward Electrocatalytic Chlorine Evolution Reactions. Journal of Physical Chemistry C, 2022, 126, 7066-7075.	3.1	20
10	Atomically-dispersed Mn-(N-C2)2(O-C2)2 sites on carbon for efficient oxygen reduction reaction. Energy Storage Materials, 2022, 49, 209-218.	18.0	26
11	Operando Converting BiOCl into Bi2O2(CO3)xCly for Efficient Electrocatalytic Reduction of Carbon Dioxide to Formate. Nano-Micro Letters, 2022, 14, 121.	27.0	15
12	Fabrication of Highâ€Quality CsBi <sub>3</sub> 1 <sub>10</sub> Films via a Gasâ€Assisted Approach for Efficient Leadâ€Free Perovskite Solar Cells. Energy Technology, 2022, 10, .	3.8	4
13	Scalable and controllable fabrication of CNTs improved yolk-shelled Si anodes with advanced in operando mechanical quantification. Energy and Environmental Science, 2021, 14, 3502-3509.	30.8	45
14	Portable wastewater treatment system based on synergistic photocatalytic and persulphate degradation under visible light. Science China Materials, 2021, 64, 1952-1963.	6.3	6
15	W18O49 nanowires-graphene nanocomposite for asymmetric supercapacitors employing AlCl3 aqueous electrolyte. Chemical Engineering Journal, 2021, 409, 128216.	12.7	72
16	Anchoring Single Copper Atoms to Microporous Carbon Spheres as Highâ€Performance Electrocatalyst for Oxygen Reduction Reaction. Advanced Functional Materials, 2021, 31, 2104864.	14.9	115
17	Distinctive O-O bond formation pathways at different electrode potentials. Matter, 2021, 4, 2615-2617.	10.0	1
18	Molten salt assisted fabrication of Fe@FeSA-N-C oxygen electrocatalyst for high performance Zn-air battery. Journal of Energy Chemistry, 2021, 61, 612-621.	12.9	33

#	Article	IF	CITATIONS
19	Real-time on-site monitoring of soil ammonia emissions using membrane permeation-based sensing probe. Environmental Pollution, 2021, 289, 117850.	7.5	5
20	Rational design of metal oxide catalysts for electrocatalytic water splitting. Nanoscale, 2021, 13, 20324-20353.	5.6	38
21	2D Electrocatalysts for Converting Earthâ€Abundant Simple Molecules into Valueâ€Added Commodity Chemicals: Recent Progress and Perspectives. Advanced Materials, 2020, 32, e1904870.	21.0	76
22	Cobalt-doped Mn3O4 nanocrystals embedded in graphene nanosheets as a high-performance bifunctional oxygen electrocatalyst for rechargeable Zn–Air batteries. Green Energy and Environment, 2020, 5, 499-505.	8.7	59
23	Fast and cost-effective room temperature synthesis of high quality graphene oxide with excellent structural intactness. Sustainable Materials and Technologies, 2020, 25, e00198.	3.3	4
24	Effects of compositional engineering and surface passivation on the properties of halide perovskites: a theoretical understanding. Physical Chemistry Chemical Physics, 2020, 22, 19718-19724.	2.8	11
25	Perovskite Microcrystals with Intercalated Monolayer MoS2 Nanosheets as Advanced Photocatalyst for Solar-Powered Hydrogen Generation. Matter, 2020, 3, 935-949.	10.0	81
26	Selective Growth of Highâ€Density Anatase {101} Twin Boundaries on Highâ€Energy {001} Facets. Small Structures, 2020, 1, 2000025.	12.0	16
27	Coexisting Singleâ€Atomic Fe and Ni Sites on Hierarchically Ordered Porous Carbon as a Highly Efficient ORR Electrocatalyst. Advanced Materials, 2020, 32, e2004670.	21.0	404
28	Guided-formation of a favorable interface for stabilizing Na metal solid-state batteries. Journal of Materials Chemistry A, 2020, 8, 7828-7835.	10.3	74
29	Transition Metal (Fe, Co, Mn) Boosting the Lithium Storage of the Multishelled NiO Anode. Energy Technology, 2020, 8, 2000008.	3.8	7
30	How Cobalt and Iron Doping Determine the Oxygen Evolution Electrocatalytic Activity of NiOOH. Cell Reports Physical Science, 2020, 1, 100077.	5.6	35
31	Phosphorus and Sulfur Coâ€Doped Cobaltous Oxide Synthesized by an Inorganicâ€Saltâ€Assisted Method: Reaction Mechanism and Electrocatalytic Application. ChemPlusChem, 2020, 85, 1602-1611.	2.8	4
32	Manganese oxides transformed from orthorhombic phase to birnessite with enhanced electrochemical performance as supercapacitor electrodes. Journal of Materials Chemistry A, 2020, 8, 3746-3753.	10.3	22
33	An inverted Bil3/PCBM binary quasi-bulk heterojunction solar cell with a power conversion efficiency of 1.50%. Nano Energy, 2020, 73, 104799.	16.0	17
34	The role of electrolyte acid concentration in the electrochemical exfoliation of graphite: Mechanism and synthesis of electrochemical graphene oxide. Nano Materials Science, 2019, 1, 215-223.	8.8	35
35	A Hollowâ€Shell Structured V <sub>2</sub> O <sub>5</sub> Electrodeâ€Based Symmetric Full Liâ€Ion Battery with Highest Capacity. Advanced Energy Materials, 2019, 9, 1900909.	19.5	51
36	Preparation of 2â€ <sup>–</sup> nm tungsten oxide nanowires based on two-phase strategy and their ultra-sensitive NO2 gas sensing properties. Journal of Colloid and Interface Science, 2019, 557, 311-317.	9.4	12

#	Article	IF	CITATIONS
37	Theoretical Understanding of Electrocatalytic Hydrogen Production Performance by Low-Dimensional Metal–Organic Frameworks on the Basis of Resonant Charge-Transfer Mechanisms. Journal of Physical Chemistry Letters, 2019, 10, 6955-6961.	4.6	15
38	Scalable Production of Graphene Oxide Using a 3D-Printed Packed-Bed Electrochemical Reactor with a Boron-Doped Diamond Electrode. ACS Applied Nano Materials, 2019, 2, 867-878.	5.0	41
39	Enhancement of photocatalytic H2 production by metal complex electrostatic adsorption on TiO2 (B) nanosheets. Journal of Materials Chemistry A, 2019, 7, 3797-3804.	10.3	11
40	Encapsulation of Plasmid DNA by Nanoscale Metal–Organic Frameworks for Efficient Gene Transportation and Expression. Advanced Materials, 2019, 31, e1901570.	21.0	130
41	Design of three-dimensional hierarchical TiO <sub>2</sub> /SrTiO <sub>3</sub> heterostructures towards selective CO <sub>2</sub> photoreduction. Inorganic Chemistry Frontiers, 2019, 6, 1667-1674.	6.0	33
42	A Yolk–Shell Structured Silicon Anode with Superior Conductivity and High Tap Density for Full Lithiumâ€ion Batteries. Angewandte Chemie - International Edition, 2019, 58, 8824-8828.	13.8	242
43	A Yolk–Shell Structured Silicon Anode with Superior Conductivity and High Tap Density for Full Lithiumâ€ion Batteries. Angewandte Chemie, 2019, 131, 8916-8920.	2.0	18
44	Room temperature production of graphene oxide with thermally labile oxygen functional groups forÂimproved lithium ion battery fabrication and performance. Journal of Materials Chemistry A, 2019, 7, 9646-9655.	10.3	27
45	Thickness Tunable Wedding-Cake-like MoS <sub>2</sub> Flakes for High-Performance Optoelectronics. ACS Nano, 2019, 13, 3649-3658.	14.6	75
46	Sulfur-doped cobalt oxide nanowires as efficient electrocatalysts for iodine reduction reaction. Journal of Alloys and Compounds, 2019, 772, 80-91.	5.5	11
47	Epitaxial Growth of Two-Dimensional Metal–Semiconductor Transition-Metal Dichalcogenide Vertical Stacks (VSe <sub>2</sub> /MX <sub>2</sub> ) and Their Band Alignments. ACS Nano, 2019, 13, 885-893.	14.6	102
48	Rapid-Heating-Triggered <i>in Situ</i> Solid-State Transformation of Amorphous TiO <sub>2</sub> Nanotubes into Well-Defined Anatase Nanocrystals. Crystal Growth and Design, 2019, 19, 1086-1094.	3.0	4
49	Wet-chemistry grafted active pyridinic nitrogen sites on holey graphene edges as high performance ORR electrocatalyst for Zn-AirAbatteries. Materials Today Energy, 2019, 11, 24-29.	4.7	23
50	Correlating electrocatalytic activities with sulfur species on sulfur-doped cobalt oxide. Materials Letters, 2019, 236, 614-617.	2.6	2
51	Tungstenâ€Doped Nanocrystalline V <sub>6</sub> O <sub>13</sub> Nanoparticles as Lowâ€Cost and Highâ€Performance Electrodes for Energy Storage Devices. Energy Technology, 2019, 7, 1801041.	3.8	10
52	Twoâ€Step Activated Carbon Cloth with Oxygenâ€Rich Functional Groups as a Highâ€Performance Additiveâ€Free Air Electrode for Flexible Zinc–Air Batteries. Advanced Energy Materials, 2019, 9, 1802936.	19.5	170
53	Space-confined growth of monolayer ReSe2 under a graphene layer on Au foils. Nano Research, 2019, 12, 149-157.	10.4	22
54	Notable hydrogen production on LaxCa1â^'xCoO3 perovskites via two-step thermochemical water splitting. Journal of Materials Science, 2018, 53, 6796-6806.	3.7	30

#	Article	IF	CITATIONS
55	Enhanced Thermochemical H2 Production on Ca-Doped Lanthanum Manganite Perovskites Through Optimizing the Dopant Level and Re-oxidation Temperature. Acta Metallurgica Sinica (English Letters), 2018, 31, 431-439.	2.9	13
56	Manipulating the Architecture of Atomically Thin Transition Metal (Hydr)oxides for Enhanced Oxygen Evolution Catalysis. ACS Nano, 2018, 12, 1878-1886.	14.6	57
57	Electrolyte Effect on Electrocatalytic Hydrogen Evolution Performance of One-Dimensional Cobalt–Dithiolene Metal–Organic Frameworks: A Theoretical Perspective. ACS Applied Energy Materials, 2018, 1, 1688-1694.	5.1	27
58	Application of chemical vapor–deposited monolayer ReSe2 in the electrocatalytic hydrogen evolution reaction. Nano Research, 2018, 11, 1787-1797.	10.4	71
59	Remarkably enhanced water splitting activity of nickel foam due to simple immersion in a ferric nitrate solution. Nano Research, 2018, 11, 3959-3971.	10.4	88
60	Correlation between Mechanical Strength of Amorphous TiO <sub>2</sub> Nanotubes and Their Solid State Crystallization Pathways. ChemistrySelect, 2018, 3, 10711-10716.	1.5	0
61	Ultrathin Nitrogenâ€Doped Holey Carbon@Graphene Bifunctional Electrocatalyst for Oxygen Reduction and Evolution Reactions in Alkaline and Acidic Media. Angewandte Chemie, 2018, 130, 16749-16753.	2.0	49
62	Ultrathin Nitrogenâ€Doped Holey Carbon@Graphene Bifunctional Electrocatalyst for Oxygen Reduction and Evolution Reactions in Alkaline and Acidic Media. Angewandte Chemie - International Edition, 2018, 57, 16511-16515.	13.8	261
63	3D graphene aerogels-supported Ag and Ag@Ag3PO4 heterostructure for the efficient adsorption-photocatalysis capture of different dye pollutants in water. Materials Research Bulletin, 2018, 105, 334-341.	5.2	47
64	Ultrathin Transition Metal Dichalcogenide/3d Metal Hydroxide Hybridized Nanosheets to Enhance Hydrogen Evolution Activity. Advanced Materials, 2018, 30, e1801171.	21.0	180
65	Enhanced Thermochemical Water Splitting through Formation of Oxygen Vacancy in La <sub>0.6</sub> Sr <sub>0.4</sub> BO <sub>3â divî/c/i&gt;</sub> (B=Cr, Mn, Fe, Co, and Ni) Perovskites. ChemPlusChem, 2018, 83, 924-928.	2.8	19
66	Sandwichâ€Like Reduced Graphene Oxide/Carbon Black/Amorphous Cobalt Borate Nanocomposites as Bifunctional Cathode Electrocatalyst in Rechargeable Zincâ€Air Batteries. Advanced Energy Materials, 2018, 8, 1801495.	19.5	65
67	Carbon-encapsulated heazlewoodite nanoparticles as highly efficient and durable electrocatalysts for oxygen evolution reactions. Nano Research, 2017, 10, 3522-3533.	10.4	27
68	Ca <sup>2+</sup> and Ga <sup>3+</sup> doped LaMnO <sub>3</sub> perovskite as a highly efficient and stable catalyst for two-step thermochemical water splitting. Sustainable Energy and Fuels, 2017, 1, 1013-1017.	4.9	37
69	Composite Yttrium arbonaceous Spheres Templated Multiâ€5hell YVO <sub>4</sub> Hollow Spheres with Superior Upconversion Photoluminescence. Advanced Materials, 2017, 29, 1604377.	21.0	51
70	One-pot, two-step synthesis and photophysical properties of 2-(5-phenylindol-3-yl)benzimidazole derivatives. RSC Advances, 2017, 7, 49374-49385.	3.6	12
71	La1-Ca Mn1-Al O3 perovskites as efficient catalysts for two-step thermochemical water splitting in conjunction with exceptional hydrogen yields. Chinese Journal of Catalysis, 2017, 38, 1079-1086.	14.0	22
72	Ni <sub>2</sub> P(O)/Fe <sub>2</sub> P(O) Interface Can Boost Oxygen Evolution Electrocatalysis. ACS Energy Letters, 2017, 2, 2257-2263.	17.4	173

#	Article	IF	CITATIONS
73	Strongly Coupled CoCr <sub>2</sub> O <sub>4</sub> /Carbon Nanosheets as High Performance Electrocatalysts for Oxygen Evolution Reaction. Small, 2016, 12, 2866-2871.	10.0	90
74	Controlled growth of CuO/Cu2O hollow microsphere composites as efficient visible-light-active photocatalysts. Applied Catalysis A: General, 2016, 521, 34-41.	4.3	47
75	Functionalization of perovskite thin films with moisture-tolerant molecules. Nature Energy, 2016, 1, .	39.5	439
76	Multi-shelled metal oxides prepared via an anion-adsorption mechanism for lithium-ion batteries. Nature Energy, 2016, 1, .	39.5	352
77	One-step solid phase synthesis of a highly efficient and robust cobalt pentlandite electrocatalyst for the oxygen evolution reaction. Journal of Materials Chemistry A, 2016, 4, 18314-18321.	10.3	97
78	Molecular engineering of Ni–/Co–porphyrin multilayers on reduced graphene oxide sheets as bifunctional catalysts for oxygen evolution and oxygen reduction reactions. Chemical Science, 2016, 7, 5640-5646.	7.4	120
79	Soft-template assisted synthesis of mesoporous CuO/Cu 2 O composite hollow microspheres as efficient visible-light photocatalyst. Materials Letters, 2016, 182, 47-51.	2.6	26
80	The surface sulfur doping induced enhanced performance of cobalt catalysts in oxygen evolution reactions. Chemical Communications, 2016, 52, 9450-9453.	4.1	47
81	Growth and in situ transformation of TiO2 and HTiOF3 crystals on chitosan-polyvinyl alcohol co-polymer substrates under vapor phase hydrothermal conditions. Nano Research, 2016, 9, 745-754.	10.4	19
82	Engineered Hematite Mesoporous Single Crystals Drive Drastic Enhancement in Solar Water Splitting. Nano Letters, 2016, 16, 427-433.	9.1	80
83	Highly Ordered Single Crystalline Nanowire Array Assembled Three-Dimensional Nb <sub>3</sub> O <sub>7</sub> (OH) and Nb <sub>2</sub> O <sub>5</sub> Superstructures for Energy Storage and Conversion Applications. ACS Nano, 2016, 10, 507-514.	14.6	81
84	Controllable synthesis of mesostructures from TiO <sub>2</sub> hollow to porous nanospheres with superior rate performance for lithium ion batteries. Chemical Science, 2016, 7, 793-798.	7.4	147
85	Switching the photocatalytic activity of g-C3N4 by homogenous surface chemical modification with nitrogen residues and vacancies. RSC Advances, 2015, 5, 21430-21433.	3.6	21
86	Adsorption and oxidation of oxalic acid on anatase TiO2 (001) surface: A density functional theory study. Journal of Colloid and Interface Science, 2015, 454, 180-186.	9.4	22
87	The search for efficient electrocatalysts as counter electrode materials for dye-sensitized solar cells: mechanistic study, material screening and experimental validation. NPG Asia Materials, 2015, 7, e226-e226.	7.9	52
88	Improved conductivity of NdFeO <sub>3</sub> through partial substitution of Nd by Ca: a theoretical study. Physical Chemistry Chemical Physics, 2015, 17, 29097-29102.	2.8	9
89	Photoelectrochemical determination of intrinsic kinetics of photoelectrocatalysis processes at {001} faceted anatase TiO <sub>2</sub> photoanodes. RSC Advances, 2015, 5, 12860-12865.	3.6	17
90	Cross-linked ZnIn 2 S 4 /rGO composite photocatalyst for sunlight-driven photocatalytic degradation of 4-nitrophenol. Applied Catalysis B: Environmental, 2015, 168-169, 266-273.	20.2	101

#	Article	IF	CITATIONS
91	An in situ vapour phase hydrothermal surface doping approach for fabrication of high performance Co <sub>3</sub> O <sub>4</sub> electrocatalysts with an exceptionally high S-doped active surface. Chemical Communications, 2015, 51, 5695-5697.	4.1	47
92	Nitrogen-Doped Carbon Nanodots@Nanospheres as An Efficient Electrocatalyst for Oxygen Reduction Reaction. Electrochimica Acta, 2015, 165, 7-13.	5.2	41
93	Rutile {111} Faceted TiO <sub>2</sub> Film with High Ability for Selective Adsorption of Aldehyde. Journal of Physical Chemistry C, 2015, 119, 17680-17686.	3.1	7
94	A fluorescent quenching performance enhancing principle for carbon nanodot-sensitized aqueous solar cells. Nano Energy, 2015, 13, 124-130.	16.0	34
95	Thiourea sole doping reagent approach for controllable N, S co-doping of pre-synthesized large-sized carbon nanospheres as electrocatalyst for oxygen reduction reaction. Carbon, 2015, 92, 339-347.	10.3	59
96	Density Functional Studies of Stoichiometric Surfaces of Orthorhombic Hybrid Perovskite CH <sub>3</sub> NH <sub>3</sub> PbI <sub>3</sub> . Journal of Physical Chemistry C, 2015, 119, 1136-1145.	3.1	73
97	Self-supported bimodal-pore structured nitrogen-doped carbon fiber aerogel as electrocatalyst for oxygen reduction reaction. Electrochemistry Communications, 2015, 51, 6-10.	4.7	51
98	Bottom-Up Enhancement of g-C3N4Photocatalytic H2Evolution Utilising Disordering Intermolecular Interactions of Precursor. International Journal of Photoenergy, 2014, 2014, 1-8.	2.5	10
99	Titania single crystals with a curved surface. Nature Communications, 2014, 5, 5355.	12.8	94
100	Structure disorder of graphitic carbon nitride induced by liquid-assisted grinding for enhanced photocatalytic conversion. RSC Advances, 2014, 4, 10676-10679.	3.6	28
101	A {0001} faceted single crystal NiS nanosheet electrocatalyst for dye-sensitised solar cells: sulfur-vacancy induced electrocatalytic activity. Chemical Communications, 2014, 50, 5569.	4.1	60
102	Directly hydrothermal growth of ultrathin MoS2 nanostructured films as high performance counter electrodes for dye-sensitised solar cells. RSC Advances, 2014, 4, 21277.	3.6	82
103	Hydrothermal Transformation of Dried Grass into Graphitic Carbonâ€Based High Performance Electrocatalyst for Oxygen Reduction Reaction. Small, 2014, 10, 3371-3378.	10.0	135
104	A self-sponsored doping approach for controllable synthesis of S and N co-doped trimodal-porous structured graphitic carbon electrocatalysts. Energy and Environmental Science, 2014, 7, 3720-3726.	30.8	198
105	Fluorineâ€Doped Porous Singleâ€Crystal Rutile TiO <sub>2</sub> Nanorods for Enhancing Photoelectrochemical Water Splitting. Chemistry - A European Journal, 2014, 20, 11439-11444.	3.3	58
106	Determination of Iodide via Direct Fluorescence Quenching at Nitrogen-Doped Carbon Quantum Dot Fluorophores. Environmental Science and Technology Letters, 2014, 1, 87-91.	8.7	74
107	Geometric structure of rutile titanium dioxide (111) surfaces. Physical Review B, 2014, 90, .	3.2	18
108	Anatase TiO2 mesocrystals with exposed (001) surface for enhanced photocatalytic decomposition capability toward gaseous styrene. Catalysis Today, 2014, 224, 216-224.	4.4	38

#	Article	IF	CITATIONS
109	Vapor-phase hydrothermal synthesis of rutile TiO2 nanostructured film with exposed pyramid-shaped (1 1 1) surface and superiorly photoelectrocatalytic performance. Journal of Colloid and Interface Science, 2014, 429, 53-61.	9.4	24
110	A highly crystalline Nb3O7F nanostructured photoelectrode: fabrication and photosensitisation. Journal of Materials Chemistry A, 2013, 1, 6563.	10.3	29
111	Nature of visible-light responsive fluorinated titanium dioxides. Journal of Materials Chemistry A, 2013, 1, 12948.	10.3	26
112	Rutile TiO2 films with 100% exposed pyramid-shaped (111) surface: photoelectron transport properties under UV and visible light irradiation. Journal of Materials Chemistry A, 2013, 1, 2646.	10.3	39
113	Vaporâ€Phase Hydrothermal Growth of Novel Segmentally Configured Nanotubular Crystal Structure. Small, 2013, 9, 3043-3050.	10.0	9
114	Crossâ€Linked g <sub>3</sub> N <sub>4</sub> /rGO Nanocomposites with Tunable Band Structure and Enhanced Visible Light Photocatalytic Activity. Small, 2013, 9, 3336-3344.	10.0	564
115	Engineering the band gap of bare titanium dioxide materials for visible-light activity: a theoretical prediction. RSC Advances, 2013, 3, 8777.	3.6	31
116	$\{001\}$ Faceted Anatase Titanium Dioxide Crystals Photoanode for Solar Cells and Photocatalysis. , 2013, , .		0
117	Low temperature solvothermal synthesis of anatase TiO2 single crystals with wholly {100} and {001} faceted surfaces. Journal of Materials Chemistry, 2012, 22, 23906.	6.7	91
118	Vertically aligned nanorod-like rutileTiO2 single crystal nanowire bundles with superior electron transport and photoelectrocatalytic properties. Journal of Materials Chemistry, 2012, 22, 2465-2472.	6.7	84
119	High-Performance Nanoporous TiO <sub>2</sub> /La <sub>2</sub> O <sub>3</sub> Hybrid Photoanode for Dye-Sensitized Solar Cells. ACS Applied Materials & Interfaces, 2012, 4, 1289-1294.	8.0	62
120	Vaporâ€Phase Hydrothermal Transformation of HTiOF <sub>3</sub> Intermediates into {001} Faceted Anatase Singleâ€Crystalline Nanosheets. Small, 2012, 8, 3664-3673.	10.0	56
121	Visible light active pure rutile TiO2 photoanodes with 100% exposed pyramid-shaped (111) surfaces. Nano Research, 2012, 5, 762-769.	10.4	57
122	Nanocrystal Cu2O-loaded TiO2 nanotube array films as high-performance visible-light bactericidal photocatalyst. Applied Microbiology and Biotechnology, 2012, 96, 1201-1207.	3.6	23
123	Single crystal α-Fe2O3 with exposed {104} facets for high performance gas sensor applications. RSC Advances, 2012, 2, 6178.	3.6	82
124	Photocatalytic Synthesis of TiO <sub>2</sub> and Reduced Graphene Oxide Nanocomposite for Lithium Ion Battery. ACS Applied Materials & Interfaces, 2012, 4, 3636-3642.	8.0	276
125	A New Vaporâ€Phase Hydrothermal Method to Concurrently Grow ZnO Nanotube and Nanorod Array Films on Different Sides of a Zinc Foil Substrate. Chemistry - A European Journal, 2012, 18, 5165-5169.	3.3	20
126	Morphological and physiological characteristics of corn (Zea mays L.) roots from cultivars with different yield potentials. European Journal of Agronomy, 2012, 38, 54-63.	4.1	96

#	Article	IF	CITATIONS
127	Directly Hydrothermal Growth of Single Crystal Nb <sub>3</sub> O <sub>7</sub> (OH) Nanorod Film for High Performance Dye‧ensitized Solar Cells. Advanced Materials, 2012, 24, 1598-1603.	21.0	86
128	A Facile Vapor-Phase Hydrothermal Method for Direct Growth of Titanate Nanotubes on a Titanium Substrate via a Distinctive Nanosheet Roll-Up Mechanism. Journal of the American Chemical Society, 2011, 133, 19032-19035.	13.7	99
129	Anatase TiO <sub>2</sub> Crystal Facet Growth: Mechanistic Role of Hydrofluoric Acid and Photoelectrocatalytic Activity. ACS Applied Materials & Interfaces, 2011, 3, 2472-2478.	8.0	108
130	A selective etching phenomenon on {001} faceted anatase titanium dioxide single crystal surfaces by hydrofluoric acid. Chemical Communications, 2011, 47, 2829.	4.1	124
131	A facile one-step preparation of hierarchically-structured TiO2 nanotube array photoanodes with enhanced photocatalytic activity. Electrochemistry Communications, 2011, 13, 1151-1154.	4.7	11
132	Rutile TiO2 microspheres with exposed nano-acicular single crystals for dye-sensitized solar cells. Nano Research, 2011, 4, 938-947.	10.4	50
133	Facile Fabrication of Anatase TiO <sub>2</sub> Microspheres on Solid Substrates and Surface Crystal Facet Transformation from {001} to {101}. Chemistry - A European Journal, 2011, 17, 5949-5957.	3.3	70
134	The fabrication of CNTs/TiO2photoanodes for sensitive determination of organic compounds. Nanotechnology, 2010, 21, 485503.	2.6	12
135	Fabrication of Highly Ordered TiO <sub>2</sub> Nanorod/Nanotube Adjacent Arrays for Photoelectrochemical Applications. Langmuir, 2010, 26, 11226-11232.	3.5	62
136	Facile Formation of Branched Titanate Nanotubes to Grow a Three-Dimensional Nanotubular Network Directly on a Solid Substrate. Langmuir, 2010, 26, 1574-1578.	3.5	20
137	Anatase TiO2 microspheres with exposed mirror-like plane {001} facets for high performance dye-sensitized solar cells (DSSCs). Chemical Communications, 2010, 46, 8395.	4.1	166
138	Direct growth of hierarchically structured titanate nanotube filtration membrane for removal of waterborne pathogens. Journal of Membrane Science, 2009, 343, 212-218.	8.2	23
139	An efficient and low-cost TiO2 compact layer for performance improvement of dye-sensitized solar cells. Electrochimica Acta, 2009, 54, 1319-1324.	5.2	326
140	High-Performance TiO <sub>2</sub> Photoanode with an Efficient Electron Transport Network for Dye-Sensitized Solar Cells. Journal of Physical Chemistry C, 2009, 113, 16277-16282.	3.1	122
141	(R)-Methyl 2-(furan-2-carboxamido)-4-methylpentanoate. Acta Crystallographica Section E: Structure Reports Online, 2007, 63, o3644-o3644.	0.2	0
142	3-(1-Methyl-1H-pyrrole-2-carboxamido)propanoic acid. Acta Crystallographica Section E: Structure Reports Online, 2006, 62, o1181-o1183.	0.2	2
143	(S)-Methyl 2-(4,5-dibromo-1H-pyrrole-2-carboxamido)-4-methylpentanoate. Acta Crystallographica Section E: Structure Reports Online, 2006, 62, o2106-o2107.	0.2	0
144	3-[(3,4,5-Tribromo-1H-pyrrol-2-ylcarbonyl)amino]propanoic acid. Acta Crystallographica Section E: Structure Reports Online, 2006, 62, o2272-o2273.	0.2	0

#	Article	IF	CITATIONS
145	3-(4-Bromo-1H-pyrrole-2-carboxamido)propanoic acid. Acta Crystallographica Section E: Structure Reports Online, 2005, 61, o1076-o1078.	0.2	1
146	N-Methyl-3-(4-bromo-1H-pyrrole-2-carbonyl)aminopropionitrile. Acta Crystallographica Section E: Structure Reports Online, 2005, 61, o1291-o1293.	0.2	0
147	3-[(4-Bromo-1-methyl-1H-pyrrol-2-ylcarbonyl)amino]propanoic acid. Acta Crystallographica Section E: Structure Reports Online, 2005, 61, o1805-o1806.	0.2	2
148	3-[(4,5-Dibromo-1-methyl-1H-pyrrole-2-carbonyl)amino]propanoic acid. Acta Crystallographica Section E: Structure Reports Online, 2005, 61, o2150-o2151.	0.2	0
149	(S)-Methyl 4-methyl-2-(1H-pyrrole-2-carboxamido)pentanoate. Acta Crystallographica Section E: Structure Reports Online, 2005, 61, o3726-o3727.	0.2	0
150	How <i>3d</i> Transition Metal Elements Determine the Oxygen Evolution Activity in Ni(OH) <sub>2</sub> Matrix. SSRN Electronic Journal, 0, , .	0.4	0
151	Atomically-Dispersed Mn-(N-C2)2(O-C2)2 Sites on Carbon for Efficient Oxygen Reduction Reaction. SSRN Electronic Journal, 0, , .	0.4	Ο